Desalination and Water Treatment
www.deswater.com

doi: 10.1080/19443994.2014.963159

56 (2015) 2284–2295
November

Taylor & Francis
Taylor & Francis Group

Preparation and characterization of thin film composite reverses osmosis membranes with wet and dry support layer

Mahdi Fathizadeh[a], Abdolreza Aroujalian[b,c,*], Ahmadreza Raisi[b,c]

[a]*Faculty of Engineering, Department of Chemical Engineering, Ilam University, Ilam 69315-516, Iran, Tel. +98 21 64543290; email: m.fathizade@aut.ac.ir (M. Fathizadeh)*
[b]*Department of Chemical Engineering, Amirkabir University of Technology (Tehran Polytechnic), Hafez Ave., P.O. Box 15875-4413, Tehran, Iran, Tel. +98 21 64543163; Fax: +98 21 66405847; email: aroujali@aut.ac.ir (A. Aroujalian), Tel. +98 21 64543125; email: raisia@aut.ac.ir (A. Raisi)*
[c]*Food Process Engineering and Biotechnology Research Center, Amirkabir University of Technology (Tehran Polytechnic), Hafez Ave., P.O. Box 15875-4413, Tehran, Iran*

Received 22 March 2014; Accepted 30 August 2014

ABSTRACT

The aim of this work is to investigate the effect of initial conditions and properties of a support layer on the performance and structure of a thin film composite (TFC) polyamide membrane. For this purpose, four different polyethersulfone (PES) support layers were prepared and the polyamide layer was coated by interfacial polymerization over these support layers in wet and dry conditions. Surface properties and morphology as well as hydrophilicity of PES support membranes and TFC membranes were examined by atomic force microscopy, field-emission scanning electron microscope, attenuated total reflectance-FTIR, and contact angle analysis, respectively. The results showed that the initial conditions of the support layer had an important role in the performance and surface properties of TFC membranes. The TFC membrane, synthesized over a wet support membrane with larger pore size and more hydrophilicity, had more water flux and lower salt rejection. The effect of wet and dry conditions on the water flux was more significant when a less hydrophilic support layer was used. It was found that the effect of support layer hydrophilicity is more effective than its pore size in wet conditions on water flux of TFC membrane, while a different trend was observed at dry conditions.

Keywords: Thin film composite (TFC); Wet and dry condition; Synthesis; Support layer properties

1. Introduction

Aromatic polyamide (PA) membranes are the most common thin film composite membranes (TFC) that have been used in water desalination [1–4]. The TFC polyamide membrane is composed of a non-woven fabric, a porous support layer, and a dense thin barrier layer. The polyamide thin layer can be synthesized via interfacial polymerization of trimesoyl chloride (TMC) and m-phenylenediamine (MPD) monomers on a porous layer which are usually prepared by the phase inversion. The effect of support layer properties on TFC membrane was investigated by some researches [4–9].

*Corresponding author.

The pore size, pore distribution, surface properties, and hydrophilicity of support layer affect the adsorption of monomers on the support surface, thus causing the formation of a deeper polyamide layer into the support pores [6,10–13]. Recently, some researchers [14,15] have been studying the role of support layer on the polyamide layer formation. The conventional PSf (polysulfone) and hydrophobic PP (polypropylene) supports were modified by plasma treatment with hydrophilic materials and used as a sub layer for interfacial polymerization of polyamide membrane by Kim and Kim [10]. They observed that the water flux, salt rejection, and chlorine resistance increased the modified support layer. Ghosh and Hoek [11] reported that the pore size, hydrophobicity, and surface properties of the support skin layer had an important effect on the performance and surface roughness of the TFC membrane. Singh et al. [12] investigated the effect of pore size of the polysulfone (PSf) support layer on the polyamide layer formation and TFC membrane performance. Their results showed that the PSf with a large pore size had the highest water and salt permeability.

Theresa et al. [14] synthesized different support layers with nanoparticles and investigated the compaction properties of these support layers in the reverse osmosis process. Tiraferri et al. [15] focused on the effect of support layer structure on the TFC membrane performance. They prepared various support layers by changing the casting conditions. Their results showed that the diameter, number, and shape of finger-like macrovoids in the support layer can change the water flux and membrane compaction of the prepared TFC membrane. Also, Susanto and Ulbricht [16] investigated the performance and characteristics of polyethersulfone (PES) membrane prepared by the phase inversion method with PVP and PEG additives. They indicated that the wet and dry PES membranes had different separation performance. Based on the Susanto and Ulbricht research, it seemed that wet and dry conditions of the PES support layer can be influenced by the characteristics and performance of the polyamide TFC membranes.

In this study, various PES support layers containing PEG 600 and PVP k90 additives were initially prepared by the phase inversion technique and characterized by atomic force microscopy (AFM), attenuated total reflectance (ATR), contact angle (CA), and field-emission scanning electron microscope (FE-SEM) analysis. Then, the TFC polyamide membranes from trimesoyl chloride (TMC) and m-phenylenediamine (MPD) monomers were fabricated over the wet and dry PES support layer. Finally, the TFC membranes were analyzed to evaluate their separation performance, hydrophilicity, surface properties, and morphology.

2. Materials and methods

2.1. Materials

N,N-dimethylacetamide (DMAc), trimesoyl chloride (TMC), m-phenylenediamine (MPD), n-hexane, sodium chloride (NaCl), and poly(ethylene glycol) (PEG 600) were purchased from Merck Co. Ltd (Darmstadt, Germany). The polyvinyl pyrrolidone (PVP-K90) was supplied by Fluka (Milwaukee, USA). Also, the used commercial polyethersulfone (Ultrason E 6020 P) was provided by BASF (Ludwigshafen, Germany).

2.2. Membrane preparation and synthesis

The four different support layers were prepared by the phase inversion technique in the PES/hydrophilic additive/DMAc/water system. The PES and hydrophilic additives (PEG600 and PVP K90) were dissolved into the DMAc solvent. The solution was mixed at room temperature over night until a homogeneous solution was obtained. Then, the PES solution was degassed by a vacuum process for 2 h. This solution was cast on a polyester non-woven fabric supported by a glass plate with a 300 μm knife gape. The glass plates were immediately immersed in a de-ionized water bath at a temperature of 25˚C. Then, the formed PES porous support layer was washed and stored in a water bath until used. There are two different initial conditions for the PES porous support layer, wet and dry. In wet conditions, the support layers remain in the water. Also, the PES porous support layer was dried at room temperature for 2 d in dry conditions.

The TFC membrane was prepared by interfacial polymerization over the PES porous support layers with wet and dry initial conditions. The PES membrane that was taped to a glass plate was placed in an aqueous solution of 2% (w/v) MPD for 2 min. The excess solution was removed from the top surface of the PES support layer by the rubber roller and was placed in the dry air blower for 4 min. Then, it was immersed in a solution of 0.1% (w/v) TMC in n-hexane at 25˚C for 1 min. The formed TFC membranes were heated in an oven at 70˚C for 6 min, washed and stored in lightproof containers at 5˚C until their use. Table 1 presents the concentration of components and experimental conditions that were used to fabricate various polyamide TFC membranes and the nomenclature to define the membrane samples.

Table 1
The experimental conditions used to fabricate various polyamide TFC membranes

Membrane sample	PES (wt %)	PEG 600 (wt %)	PVP K90 (wt %)	DMAc (wt %)	Initial condition
AW	20	–	–	80	Wet
AD	20	–	–	80	Dry
BW	15	5	–	80	Wet
BD	15	5	–	80	Dry
CW	15	–	5	80	Wet
CD	15	–	5	80	Dry
DW	15	2.5	2.5	80	Wet
DD	15	2.5	2.5	80	Dry

2.3. Membrane characterization

A cross-flow flat-sheet membrane module was used for measuring the flux and salt rejection of the TFC membranes. The filtration area, operating pressure, and temperature are 35 cm^2, 176.4 psi (~12 bar) and 25 ℃, respectively. The same procedure was used to determine the separation performance of PES porous membrane at an operating pressure of 29.4 psi (~2 bar). The details of the RO membrane setup used in the experiments are presented elsewhere [17]. The volumetric pure water flux, J_v, was calculated using the following equation:

$$J_v = \frac{v}{A \times t} \tag{1}$$

where v is the volume of the collected permeate (l), A is the membrane area (m^2), and t is the time duration of the experiment (h). Salt rejection (R) of TFC membranes was calculated by measuring the rejection of 2,000 ppm of NaCl which was analyzed with the conductivity of the feed and product solutions using a calibrated conductivity meter (DiST®4 (HI98304), HANNA instruments®, Inc., Italy) as follows:

$$R = 1 - \frac{C_p}{C_f} \tag{2}$$

Mean pore radius, r_p (μm), could be experimentally determined by the Guerout–Elford–Ferry equation [18]:

$$r_p = \sqrt{\frac{(2.9 - 1.75\varepsilon) \times 8\eta\ell Q}{\varepsilon \times \Delta P}} \tag{3}$$

where η is the water viscosity (8.9×10^{-4} Pa s), ℓ is the membrane thickness (m), Q is the volume of the permeate water per unit time ($m^3\ s^{-1}$), and ΔP is the operating pressure (0.2 MPa). The equilibrium water content of the PES membrane before and after drying at room temperature was calculated as follows:

$$\text{Equilibrium water content}\,(\%) = \frac{W_w}{W_d} \times 100 \tag{4}$$

where W_w and W_d are the wet and dry membrane weights (g), respectively. The PES porous support layer was separated from the polyester layer and weighed (W_w) and dried for 24 h in the desiccators. After completion of drying, the dried membrane was weighed and the value was recorded as W_d. Eq. (4) was also used to determine the equilibrium water content in dry conditions. To obtain W_w in dry conditions, the PES membrane was placed in the water for 24 h and weighed (W_w), and similarly W_d was measured to the wet conditions.

The PES membrane porosity which has an important role on permeation and separation performance was determined as [19]:

$$\textit{Porosity}\,(\varepsilon) = \frac{W_w - W_d}{\rho_w \times V} \tag{5}$$

where ρ_w and V are the density of pure water (kg/m^3) and the membrane volume in the wet state (m^3), respectively.

The shrinkage of the PES porous support layer was calculated by measuring the thickness of wet and dry membranes by the following equation:

$$\text{Sh}\,\% = \left(1 - \frac{L_1}{L_0}\right) \times 100 \tag{6}$$

where L_1 and L_0 are the thickness of membrane after and before drying, respectively. Furthermore, the shrinkage of TFC membranes was characterized by

measuring the thickness of the TFC membrane before (L_0) and after (L_1) flux measurement tests which can be calculated according to Eq. (6). All measurements were repeated three times and the average values were reported.

The presence of functional groups on the membrane surfaces and the polyamide layer thickness were detected by attenuated total reflection-Fourier transform infrared spectroscopy (ATR-FTIR) analysis. The ATR-FTIR instrument used consisted of a Nicolet Nexus 670 spectrometer (Thermo-Nicolet, Instrument Co., Madison, WI, USA), which coupled to a ZnSe ($n_1 = 2.43$) prism as an internal reflection element was fixed at a 60˚ angle of incidence with 4 cm^{-1} resolution over a wave number range of 4,000–600 cm^{-1}. A 2 × 6 cm sample of the dried TFC membranes was used in ATR analysis for detecting the presence of functional groups on the membrane surfaces and the polyamide layer thickness [20]. The top layer thickness of the TFC membranes can be calculated by using the IR absorbance peak at a wave number of 1,660 cm^{-1}, which shows the C–N polyamide band [17,20].

The cross-section pictures and surface morphology of the PES porous support layer and TFC membranes were analyzed by FESEM (Hitachi, model S-4160, Japan). The sample of the cross section was prepared by freezing and breaking the membrane sample in liquid nitrogen. The membrane samples were dried and stuck on a conducting sample holder with double-sided copper tape. The prepared samples were coated under vacuum with a ~10–20 nm thin layer of Au by a sputtering system.

An AFM (NanoEducator, NT-MDT Co., Zelenograd, Russia) with a spatial resolution of ~2 nm in z direction was used to determine surface roughness (RMS) and relative surface area (Δ) for the support membranes and polyamide films. The instrument was calibrated by standard samples (TGG1 and TGX1, NT-MDT Co., Zelenograd, Russia). Dried membrane samples were fixed on a holder using double-side tape and 10 μm × 10 μm areas were scanned by semi-contact mode in the air [21].

The water CA of the membrane surface was measured using an optical CA measurement system (OCA-20, dataphysics GmbH, Filderstadt, Germany) at 25˚C. Five microliter of de-ionized water was dropped on the membrane surface by a micro-syringe. The CA of several locations of the membrane surface was measured and the average of values was reported as CA for one membrane sample.

Another parameter that can represent a film's hydrophilicity is the solid–liquid interfacial free energy ($-\Delta G_{SL}$) [22]. The interfacial free energy can be determined using:

$$-\Delta G_{SL} = \gamma_L \left(1 + \frac{\cos\theta}{\Delta}\right) \quad (7)$$

where θ, Δ, and γ_L that equal to 72.8 m J/m^2 for pure water at 25˚C are the average CA, relative surface area, and the liquid surface tension, respectively. In the same CA, the smoother surface has higher interfacial free energy and is more hydrophilic. The maximum of the interfacial free energy is $2\gamma_L$ as CA is 0˚ and relative surface area (Δ) is 1 [20,23].

3. Results and discussion

3.1. PES porous layer

3.1.1. Support layer performance

The results of characterization tests on the PES porous membranes are summarized in Table 2. As shown in this table, the water flux in the wet condition was higher than dry condition. This is due to a decrease in the pore size and water content of the membrane after drying. Also, addition of PEG to the membrane samples increased the water permeability through the membrane for both wet and dry conditions. The hydrophilic PEG additive increases the number and size of macrovoids in the membrane structure [24]; therefore, the water molecule can easily pass through the membrane and the permeation flux increases. In wet conditions, membrane sample C has higher water flux than sample A due to the presence of PVP in the membrane structure; however, a reverse effect was observed after drying. There are different results about PVP adding to the PES ultrafiltration membrane in the literature [16,25]. For example, Susanto and Ulbricht [16] reported that PVP increased the water flux in wet condition and decreased the water permeation after drying, but Miyano et al. [25] observed that PVP decreased the water permeability. The flux ratios between the wet and dry membranes were 5.68, 5.8, 53.15 and 32.38 for membrane type A, B, C, and D, respectively. These results show that PVP as a hydrophilic additive had the highest effect on the performance of the dried membrane. The absence of impregnation may contribute to this very large decrease in the flux after drying [16].

3.1.2. Support layer characterization

The CA of the support layer in membrane samples of A, B, and C was 62.5˚, 58.5˚ and 64.5˚, respectively. The membrane type B with PEG 600 as a hydrophilic additive had higher CA than type A, because the CA value is influenced not only by membrane material

Table 2
The separation performance and surface properties of different PES porous support layers

Membrane sample	CA	RMS (nm)	Flux (l/m^2 h)	J_v (wet)/ J_v (dry)	r_p (nm)	L* (μm)	Sh (%)**	ΔG (m J/m^2)	Water content (%)	Porosity
AW	–	–	413.56	5.68	37.34	86	12.79	–	71.42	0.51
AD	62.5 ± 2.2	12.3 ± 2	72.87		25.42	75		93.19	44.76	0.21
BW	–	–	1,702.14	5.80	61.12	76	10.53	–	67.65	0.62
BD	64.5 ± 2	8.03 ± 1.2	293.52		24.86	68		98.95	66.67	0.59
CW	–	–	607.53	53.15	34.94	107	21.50	–	76.02	0.79
CD	58.5 ± 1.7	10.12 ± 0.7	11.43		9.06	84		99.06	51.24	0.28
DW	–	–	1,054.70	32.38	44.46	86	15.12	–	73.76	0.73
DD	60 ± 0.5	9.52 ± 0.9	32.57		10.65	73		101.95	62.82	0.44

*L = thickness of porous film.
**Sh = Shrinkage.

but also by surface porosity [11,16,23]. Besides, the solid–liquid interfacial free energy was used to evaluate the relative hydrophilicity of membranes [23,26]. The results indicated that an addition of hydrophilic PEG and PVP enhanced the interfacial free energy. Similar results were observed by other researchers [27,28].

The thickness of the membrane samples had a different behavior with PEG 600 and PVP K90. PEG 600 that has low molecular weight decreased final thickness of the support membrane; in contrast, PVP K90 increased the membrane thickness [25]. Also, drying of the PES membranes led to a decrease in the membrane thickness and the highest shrinkage was observed for membrane sample C. Decreasing the membrane volume during the drying process affected the membrane structure and reduced the pore volume. It has been previously reported that shrinkage had an effect on the membrane porosity [16,29]. As shown in Table 2, membrane drying resulted in a decrease in the average pore size for all PES membrane samples. Therefore, a decline in the permeation flux after membrane drying can be related to the membrane shrinkage and decrease in the porosity (Table 2). It was observed that the PES membranes with hydrophilic additives had more porosity and water content than those without additives, so addition of PEG and PVP led to higher water flux. The significant reduction in the porosity of membrane type C in dry condition may be a reason for its low water flux.

The cross section FESEM images of the PES membranes and the pore size (r_p) are shown in Fig. 1 and Table 2, respectively. It is found that the pore size of the surface became bigger and the distance from the top surface to the starting point of the macrovoid formation became larger as PEG and PVP were added to the PES membrane in the wet conditions. Increasing the pore size by adding PEG 600 agrees with the results reported by Idris et al. [24]. The pore size of the type C membrane is decreased by adding the PVP to PES membrane, which can be compared with the findings of Miyano et al. [30]. They reported that the pore size of PES, without any additive, deceases from 29.5 to 16.2 nm as the PVP is added to PES UF membrane. Fig. 1 and Table 2 show that the thickness of four PES membranes which were measured by a micrometer is in order of B < D < A < C. Idris et al. [24] showed that the asymmetric layer thickness decreases as PEG is added to the casting solution. Also, Miyano et al. [30] reported that adding PVP to the PES UF membrane increased the final thickness of the formed membrane. Also, the morphology of the support membrane has a strong effect on the water flux and compaction under pressure (shrinkage) [14,15]. The macrovoids size and shape as well as the thickness of support membranes changed when PEG and PVP were added into the cast solution (Fig. 1). The membranes containing PVP (type C and D) had uniform finger-like macrovoids and a relatively dense skin layer on the PES support membrane (Fig. 1(c) and (d)). On the other hand, the PEG 600 decreased the membrane thickness and cross sectional finger size (Fig. 1(b)), which improves the water flux and compaction properties [24].

3.2. TFC membranes

3.2.1. Separation performance

As shown in Table 3, the separation performance of formed TFC membranes significantly depends on the type of support membrane and its initial condition. The water and salt permeability in the wet condition were higher than initial dry conditions in all

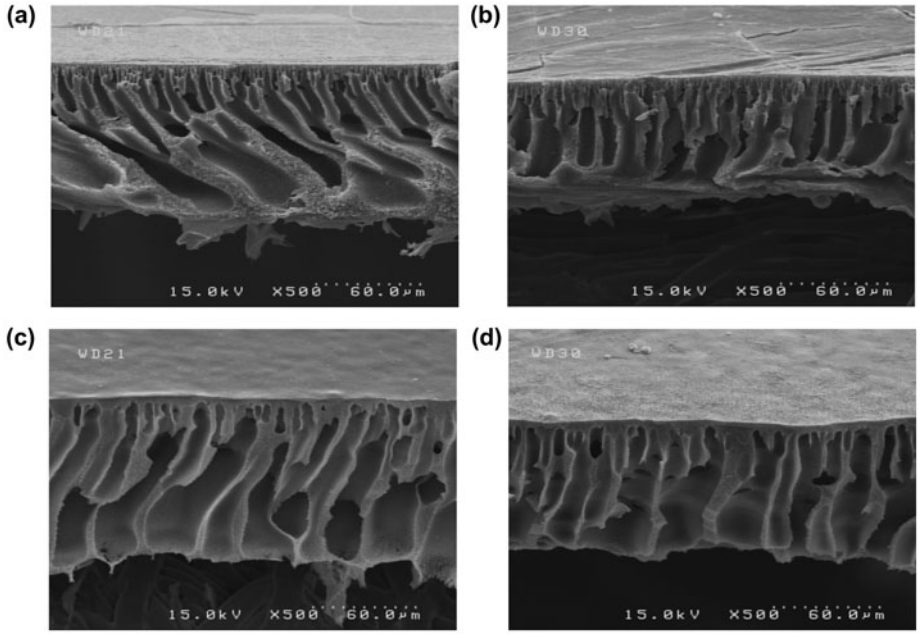

Fig. 1. Cross section FESEM image of the PES support layers: (a) type A (PES 20%), (b) type B (PES 15%-PEG 5%), (c) type C (PES 15%-PVP 5%), and (d) type D (PES 15%-PVP 2.5%-PEG 2.5%).

Table 3
The water flux, NaCl rejection, RMS roughness, CA, and interfacial free energy of the fabricated TFC membranes

	Flux (l/m^2 h)	Rejection (%)	Contact angel	RMS (nm)	ΔG (m J/m^2)
AD	3.011	85.791	56.4684	78.6127	100.219
AW	8.88836	82.313	57.8881	56.6458	102.727
BD	9.73302	86.2657	40.8002	67.7569	110.059
BW	12.4382	62.1556	40.0198	60.8562	117.905
CD	6.73	96.8459	59.6674	68.1266	101.335
CW	10.4854	76.2051	53.5886	53.6149	97.2309
DD	9.41748	85.3221	47.082	67.0132	104.166
DW	9.03569	83.6933	56.3128	56.3405	102.182

support membranes. The hydrophilic support layer with large pore size has the highest water flux in both wet and dry conditions. The water flux under wet and dry conditions decreased in an order of BW > AW > CW > DW and BD > DD > CD > AD. The results of water flux in wet conditions show that the pore size of the support layer was more effective than hydrophilicity. In the same pore size, the TFC membrane formed on the more hydrophilic support layer had more water and salt permeability. In the wet condition, the pore size had an important role in the polyamide formation over the support surface due to the wet surface of the support layer. These results are in good agreement with previous researches. It is reported by Ghosh and Hoek [11] and Singh et al. [12] that the support membrane with the largest pore size produced a polyamide TFC membrane with the highest flux and low salt rejection.

The pore size of support layers decreased in the dry condition which caused a significant reduction in the water and salt permeability of the TFC membranes. The hydrophilicity of the support layer is more effective than pore size in the dry condition (Table 3). A comparison between the salt rejection and water flux of type A and B support layers clearly shows that the TFC membrane that fabricated over the hydrophilic support layer had better performance. Furthermore, type B support layer had a larger pore size than type C and D at nearly the same hydrophilicity which caused more water flux for the B type

TFC membrane than the C and D types TFC membranes at dry conditions.

The water flux of type A membrane formed on a wet support was 8.98 l/m^2 h while this value for that membrane formed on a dry support was 2.87 l/m^2 h. This reduction in the water flux can be related to a decrease in pore size as well as enhancement in the hydrophilicity effect as the initial condition of support layer was changed from wet to dry. The results of the TFC membranes performance showed that the TFC membrane formed over the dried support layer has less water and salt permeability than wet conditions. Kim and Kim [10] reported that increasing the hydrophilicity of the support layer causes an improvement in the performance of TFC membrane, which can be concluded from comparing AD and CD performance of the TFC membranes.

The common phenomenon which affects the membrane permeability and causes compression of the membrane structure is mechanical deformation of the solid polymer under the transmembrane pressure during the application of polymeric membranes [14,15]. Tiraferri et al. [15] showed that the diameter, number, and shape of finger-like macrovoids in the support layer can change the prepared TFC membrane water flux. The TFC membranes have support with a dense skin layer over finger-like macrovoids (e.g. support membrane type C and D) exhibited lower water flux than the membranes have support with a porous skin layer over finger-like macrovoids (e.g. membrane support layer type B). The macrovoids diameter increased as PVP was added to the PES support which decreases the compaction resistance in the type D and C. On the other hand, PEG increases the number of macrovoids and decreases their diameter; therefore the TFC membranes formed on the type B support layer had a low compaction under the pressure as showed in Table 4. The separation performance results of the TFC membranes showed that the AD membrane sample with the lowest shrinkage (3.33%) and CW samples with highest shrinkage (50.47%) had about 6.34 and 36.78% reduction in the water flux after 4 h, respectively.

3.2.2. ATR analysis

The ATR analysis of the TFC polyamide membranes formed at wet and dry conditions is shown in Fig. 2. The peaks of C=O stretch, C–N stretch, polyamide aromatic ring breathing, and amide are observed at wave numbers of 1,660, 1,609, 1,547, and 786 cm^{-1}, respectively. The skeletal aliphatic C–C/aromatic hydrogen bending and aliphatic C–H rocking of polyamide appeared at 1,200–900 cm^{-1}. The C=O stretching of carboxylic acids in the polyamide TFC membrane spectrum peak clearly appeared at 1,720 cm^{-1}, which presents a pendant carboxylic acid groups in the polyamide films [13,31]. When the acid chloride group of an available branch reacts with an amine group, a totally cross-linked structure of polyamide is formed on the support layer. Also, a linear structure with a pendant carboxylic acid from the hydrolysis of one acyl chloride group of the trimesoyl chloride can remain in the polyamide structure [3,32,33].

In order to investigate the cross-linking of the polyamide synthesized on different support layers in wet and dry conditions, the ratio of acid (–COOH) content in the film at 1,720 cm^{-1} relative to the amide I (–COONH–) band at 1,660 cm^{-1} was used and the results are shown in Table 4. Interfacial polymerization between MPD and TMC occurs predominantly in the organic phase due to the relatively low solubility of TMC in water. If these acid chlorides can react with more incoming MPD monomers, they will result in a denser and more cross-linked film with a lower acid content. In other words, the absorbance ratio of (–COOH)/(–COONH–) in the polyamide layer film can represent the degree of cross-linking [13].

Also, the thickness of polyamide layer formed over the different support layer membranes were estimated by the intensities of characteristic IR bands of polyamide groups as shown in Table 4. The approximated film thicknesses based on the absorbance values of the 1,660 cm^{-1} band (amide C–N stretching band) are between 150 nm and 300 nm. The maximum penetration depth at 1,660 cm^{-1} is about 650 nm for

Table 4
The polyamide layer thickness, shrinkage, and (–COOH)/(–COONH–) ratio of the TFC membranes

Membrane sample	AD	AW	BD	BW	CD	CW	DD	DW
Compaction (%)	3.33	22.48	15.44	29.82	32.53	50.47	22.60	27.33
L (μm)	283.97	258.4	255	225.37	205.6	236.3	164.14	193.6
(–COOH)/(–COONH–)	0.0833	0.1744	0.214	0.128	0.081	0.138	0.072	0.149

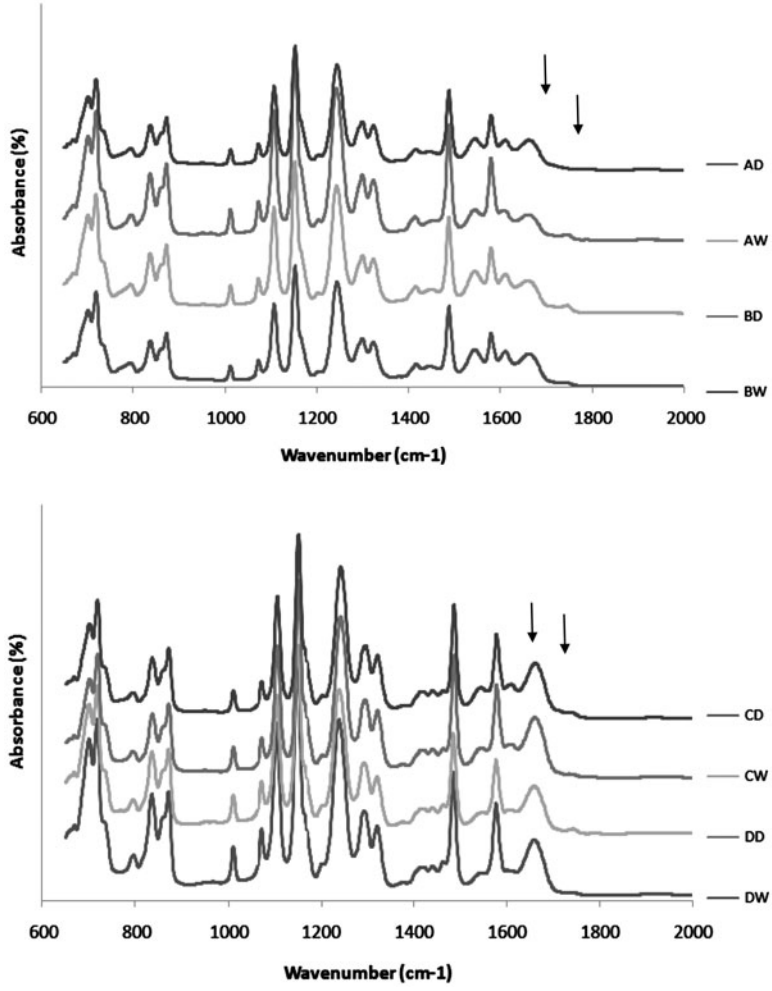

Fig. 2. ATR-FTIR spectrum of the fabricated TFC polyamide.

ATR-FTIR operation, which is more than polyamide layer thickness; therefore ATR-FTIR is suitable to estimate an accurate value of film thicknesses in all TFC membranes.

The variation of film thickness, hydrophilicity, and cross-linking of polyamide layer can change the water flux and salt rejection of TFC membrane performances. Generally, the water and salt permeability decreased as the polyamide layer thickness or cross-linking increased. Also, polymer films with higher extents of cross-linking tend to be less hydrophilic due to their limited ability to swell and absorb water [23]. The CA and (–COOH/–COONH–) ratio results confirmed this fact. As the thickness and cross-linking increased simultaneously in the AD TFC membrane, the water and salt rejection significantly decreased.

In the initial stages of the MPD-TMC polymerization, MPD molecules diffuse from the water phase into the organic side of the interface and react with the TMC molecules which result in the production of initial polyamide film with many pendant acid chlorides [31,34]. The adsorbed MPD monomers over the support layer pore surfaces can react with these acid chlorides, resulting in a denser and more cross-linked film [31]. The wet condition of support layer due to increase pore size and decrease MPD concentration on the pore is compared with dry conditions which enhance acid content on the formed TFC membrane (Table 4). Also, the hydrogen bonding between MPD and hydrophilic bands of additive limit the diffusion rate of MPD into the reaction zone. As the reaction zone is near the surface which can occur in the hydrophilic support layer, some TMC may diffuse into the pores or support surface which forms a deep polyamide within the pores creating a longer effective film thickness for water permeation.

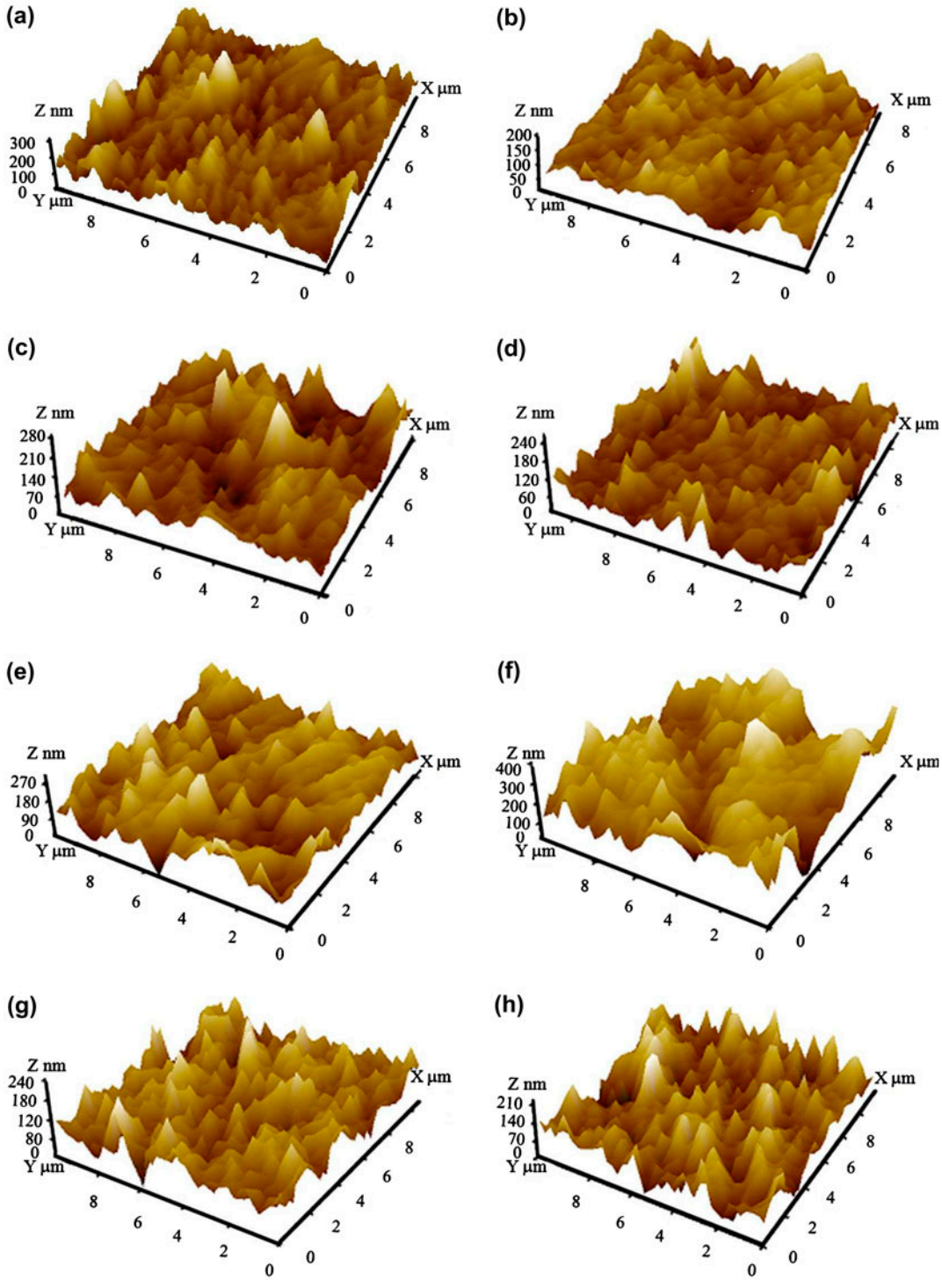

Fig. 3. AFM images of the TFC membranes: (a) AD, (b) AW, (c) BD, (d) BW, (e) CD, (f) CW, (g) DD, and (h) DW.

3.2.3. Surface characterization

Table 3 and Fig. 3 show the surface roughness (RMS) and the AFM image of TFC membranes in wet and dry conditions. It can be seen from the AFM images that the TFC composite membranes in the wet condition were smoother than the dry condition and thus it appears that the wet condition incorporates

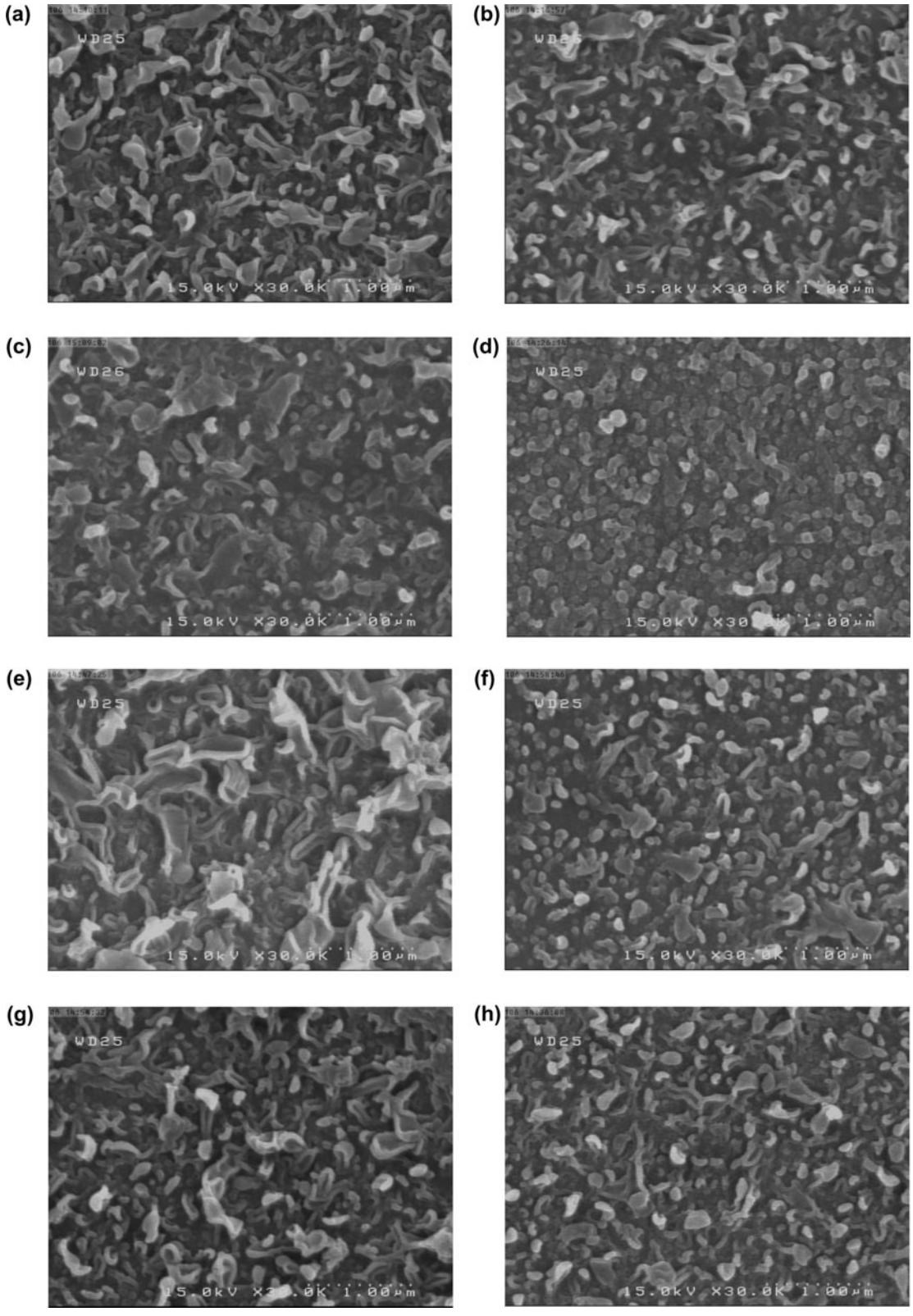

Fig. 4. FESEM images of the surface morphology of the fabricated TFC membranes: (a) AW, (b) AD, (c) BW, (d) BD, (e) CW, (f) CD, (g) DW, and (h) DD.

lower roughness to the membrane surface compared to dry conditions. The surface roughness value of membranes indicate the highest roughness for the AD membrane sample and the lowest RMS value for the CW and DW membranes. The higher roughness for the membranes formed at dry conditions could be due to a greater degree of cross-linking.

The FESEM images of the TFC membranes prepared using interfacial polymerization on different support membranes are shown in Fig. 4. The surface morphology of the polyamide TFC membranes formed on the PES support layer without additives in the wet and dry conditions is shown in Fig. 4(a) and (b), which also shows the surface morphology of the AW TFC membrane changes from leaf-like to nodular morphology in the dry condition. In the wet condition, the formed TFC membranes exhibited more leaf-like folds on its surface in all types of support membranes. The DD and CD TFC membranes have approximately the same surface morphology which appears similar to a nodule. Also, the DD TFC membrane which has different morphology with other TFC membranes shows a ridge-and-valley morphology. The hydrophilicity, pore size, and initial condition of support can affect the TFC membranes morphology and surface roughness. The hydrophilicity and lager pore size of the support membrane is due to MPD diffuse into the pore and produces a smoother surface with leaf-like morphology which is clearly observed in the BW TFC membrane. Also, the support layer with small pore size produced a TFC membrane with nodular morphology, as shown in Fig. 4(f) and (h).

4. Conclusions

The performance results of support PES layers indicated that the water flux of wet membranes is significantly more than dry membranes because of the higher pore size and porosity of wet membranes. Besides, the PES support membrane without additives had the lowest water flux decline and shrinkage from wet to dry conditions comparing with the PES support layer with PEG and PVP.

The prepared TFC membranes over PES support layer show widely varying separation performance, surface properties, and compaction ability. In dry conditions, the hydrophilicity of the PES support layers is more effective than pore size on TFC membrane performance. The TFC membrane, was polymerized over the dry support layer, has a thinner polyamide layer, less hydrophilicity, rougher polyamide membrane, and a greater degree of cross-linking. On other hand, the fabricated TFC membranes over the wet support layer had more water flux, lower degree of cross-linking, and less rough surface. Finally, it can be concluded that the wet and dry conditions of support layer had significant effects on the performance and characterizations of TFC membranes and these parameters should be optimized to achieve the desired composite membrane.

Acknowledgments

The authors gratefully acknowledge the financial support of SANAYEE NOVIN plans of Iranian Industry, Mine and Trade Ministry.

References

[1] P.L. Kah, C.A. Tom, M. Davide, A review of reverse osmosis membrane materials for desalination-development to date and future potential, J. Membr. Sci. 370 (2011) 1–22.
[2] A.P. Rao, N.V. Desai, R. Rangarajan, Interfacially synthesized thin film composite RO membranes for seawater desalination, J. Membr. Sci. 124 (1997) 263–272.
[3] Y.M. Feng, X.L. Chang, W.H. Wang, R.Y. Ma, Separation of galacto-oligosaccharides mixture by nanofiltration, J. Taiwan Inst. Chem. Eng. 40 (2009) 326–332.
[4] S. Yu, M. Liu, X. Liu, C. Gao, Performance enhancement in interfacially synthesized thin-film composite polyamide-urethane reverse osmosis membrane for seawater desalination, J. Membr. Sci. 342 (2009) 313–320.
[5] E.L. Wittbecker, P.W. Morgan, Interfacial polycondensation. I, J. Polym. Sci., Part A: Polym. Chem. 34 (1996) 521–529.
[6] I. Sadeghi, A. Aroujalian, A. Raisi, B. Dabir, M. Fathizadeh, Surface modification of polyethersulfone ultrafiltration membranes by corona air plasma for separation of oil/water emulsions, J. Membr. Sci. 430 (2013) 24–36.
[7] V. Freger, Kinetics of film formation by interfacial polycondensation, Langmuir 21 (2005) 1884–1894.
[8] A. Soroush, J. Barzin, M. Barikani, M. Fathizadeh, Interfacially polymerized polyamide thin film composite membranes: Preparation, characterization and performance evaluation, Desalination 287 (2012) 310–316.
[9] I.C. Kim, J. Jegal, K.H. Lee, Effect of aqueous and organic solutions on the performance of polyamide thin-film-composite nanofiltration membranes, J. Polym. Sci., Part B: Polym. Phys. 40 (2002) 2151–2163.
[10] H.I. Kim, S.S. Kim, Plasma treatment of polypropylene and polysulfone supports for thin film composite reverse osmosis membrane, J. Membr. Sci. 286 (2006) 193–201.
[11] A.K. Ghosh, E.M.V. Hoek, Impacts of support membrane structure and chemistry on polyamide-polysulfone interfacial composite membranes, J. Membr. Sci. 336 (2009) 140–148.
[12] P.S. Singh, S.V. Joshi, J.J. Trivedi, C.V. Devmurari, A. PrakashRao, P.K. Ghosh, Probing the structural variations of thin film composite RO membranes obtained

by coating polyamide over polysulfone membranes of different pore dimensions, J. Membr. Sci. 278 (2006) 19–25.
[13] M. Fathizadeh, A. Aroujalian, A. Raisi, Effect of lag time in interfacial polymerization on polyamide composite membrane with different hydrophilic sub layers, Desalination 284 (2012) 32–41.
[14] M. Theresa, M. Pendergast, J.M. Nygaard, A.K. Ghosh, E.M.V. Hoek, Using nanocomposite materials technology to understand and control reverse osmosis membrane compaction, Desalination 261 (2010) 255–263.
[15] A. Tiraferri, N.Y. Yip, W.A. Phillip, J.D. Schiffman, M. Elimelech, Relating performance of thin-film composite forward osmosis membranes to support layer formation and structure, J. Membr. Sci. 367 (2011) 340–352.
[16] H. Susanto, M. Ulbricht, Characteristics, performance and stability of polyethersulfone ultrafiltration membranes prepared by phase separation method using different macromolecular additives, J. Membr. Sci. 327 (2009) 125–135.
[17] M. Fathizadeh, A. Aroujalian, A. Raisi, Effect of added NaX nano-zeolite into polyamide as a top thin layer of membrane on water flux and salt rejection in a reverse osmosis process, J. Membr. Sci. 375 (2011) 88–95.
[18] J.F. Li, Z.L. Xu, H. Yang, C.D. Feng, J.H. Shi, Hydrophilic microporous PES membranes prepared by PES/PEG/DMAc casting solutions, J. Appl. Polym. Sci. 107 (2008) 4100–4108.
[19] B. Chakrabarty, A.K. Ghoshal, M.K. Purkait, Effect of molecular weight of PEG on membrane morphology and transport properties, J. Membr. Sci. 309 (2008) 209–221.
[20] C.K. Kim, J.H. Kim, I.J. Roh, J.J. Kim, The changes of membrane performance with polyamide molecular structure in the reverse osmosis process, J. Membr. Sci. 165 (2000) 189–199.
[21] V.A. Bykov, V.N. Vasil'ev, A.O. Golubok, Minilaboratory for education and the first steps of R&D in nanotechnology based on the nanoeducator scanning probe microscope, Nanotechnol. Russ. 4 (2009) 530–539.
[22] M.L. Lind, A.K. Ghosh, A. Jawor, X. Huang, W. Hou, Y. Yang, E.M.V. Hoek, Influence of zeolite crystal size on zeolite-polyamide thin film nanocomposite membranes, Langmuir 25 (2009) 10139–10145.
[23] N.Y. Yip, A. Tiraferri, W.A. Phillip, J.D. Schiffman, M. Elimelech, High performance thin-film composite forward osmosis membrane, Environ. Sci. Technol. 44 (2010) 3812–3818.
[24] A. Idris, N.M. Zain, M.Y. Noordin, Synthesis, characterization and performance of asymmetric polyethersulfone (PES) ultrafiltration membranes with polyethylene glycol of different molecular weights as additives, Desalination 207 (2007) 324–339.
[25] T. Miyano, T. Matsuura, S. Sourirajan, Effect of polyvinylpyrrolidone additive on the pore size and the pore size distribution of polyethersulfone (Victrex) membranes, Chem. Eng. Commun. 119 (1993) 23–39.
[26] R.N. Wenzel, Surface roughness and contact angle, J. Phys. Colloid Chem. 53 (1949) 1466–1467.
[27] N.A. Ochoa, P. Prádanos, L. Palacio, C. Pagliero, J. Marchese, A. Hernández, Pore size distributions based on AFM imaging and retention of multidisperse polymer solutes, J. Membr. Sci. 187 (2001) 227–237.
[28] J. Marchese, M. Ponce, N.A. Ochoa, P. Prádanos, L. Palacio, A. Hernández, Fouling behaviour of polyethersulfone UF membranes made with different PVP, J. Membr. Sci. 211 (2003) 1–11.
[29] L. Wu, J. Sun, Q. Wang, Poly(vinylidene fluoride)/polyethersulfone blend membranes: Effects of solvent sort, polyethersulfone and polyvinylpyrrolidone concentration on their properties and morphology, J. Membr. Sci. 285 (2006) 290–298.
[30] T. Miyano, T. Matsuura, S. Sourirajan, Effect of polyvinylpyrrolidone additive on the pore size and the pore size distribution of polyethersulfone (Victrex) membranes, Chem. Eng. Commun. 119 (1993) 23–39.
[31] Y. Jin, Z. Su, Effects of polymerization conditions on hydrophilic groups in aromatic polyamide thin films, J. Membr. Sci. 330 (2009) 175–179.
[32] G.M. Geise, H.S. Lee, D.J. Miller, B.D. Freeman, J.E. Mcgrath, D.R. Paul, Water purification by membranes: The role of polymer science, J. Polym. Sci., Part B: Polym. Phys. 48 (2011) 1685–1718.
[33] J.S. Louie, I. Pinnau, I. Ciobanu, K.P. Ishida, A. Ng, M. Reinhard, Effects of polyether-polyamide block copolymer coating on performance and fouling of reverse osmosis membranes, J. Membr. Sci. 280 (2006) 762–770.
[34] S.M. Aharoni, Rigid aromatic fractal polyamides, Polym. Adv. Technol. 6 (1995) 373–382.